Zhanpeng Fang
Liukai Zhao
Yanqiu Xiao ✉
Jiaqi Qi
Guangzhen Cui
Lianhui Jia
Wei Xiao

https://doi.org/10.21278/TOF.502075425
ISSN 1333-1124
eISSN 1849-1391

LIGHTWEIGHT DESIGN OF FORKLIFT TRUCK BOOM CROSS-SECTION BASED ON MULTI-LEVEL OPTIMISATION

Summary

To reduce the material consumption of the telescopic boom of forklift trucks, a multi-level optimisation lightweight design approach for the boom is proposed. Based on actual loading conditions, a mechanical model of the boom cross-section is established, and the design is optimised through topology optimisation. By analysing the impact of element size, volume fraction, and threshold values on the performance of the telescopic boom's cross-section, the optimal topology of its configuration is obtained. The parametric model of the boom is reconstructed based on the topology optimisation result. With the minimisation of the boom mass as the objective, and both stress and deformation as constraints, the cross-sectional parameters of the boom are optimised. The design variables are sampled by the Optimal Space-Filling (OSF) design method, and the Kriging surrogate model is used to construct a high-precision model, thereby enhancing computational efficiency and ensuring accuracy. The Multi-Objective Genetic Algorithm (MOGA) is used to solve the optimisation model and identify the optimal solution. Upon validation, the optimised boom not only reduces the mass by 8.44%, but also improves its torsional stiffness, effectively reduces the material usage, and has important guiding significance for the lightweight design of telescopic booms.

Key words: *telescopic boom forklift; topology optimisation; parameter optimisation; lightweight design; MOGA*

1. Introduction

Telescopic boom forklifts, a type of special vehicle, are extensively used in modern industrial and urban construction due to their strong manoeuvrability, diverse operational capabilities, and broad working range [1]. They not only efficiently handle materials in confined spaces but can also perform high-altitude tasks. During the operation of telescopic boom forklifts, the telescopic boom, as the primary load-bearing component, often leads to accidents due to insufficient strength and stiffness. Traditional telescopic boom designs rely on the designer's experience and intuition, leading to overly conservative designs which add unnecessary material and increase cost.

Focusing on the lightweight design of a telescopic boom, both domestic and international scholars have conducted extensive research. Guo et al. [2] applied a topology optimisation approach based on mobile deformable components (MMCs) to the design of thin-walled beam sections, significantly improving the stiffness-to-mass ratio while maintaining structural performance. Shimoda et al. [3] proposed a parameter-free optimisation method to optimise the cross-sectional shape of thin-walled structures using the H1 gradient method, minimising the cross-sectional perimeter while maintaining constraints on cross-sectional properties. Ji et al. [4] employed a collaborative optimisation strategy, combining NURBS curve modelling with finite element analysis techniques, to comprehensively optimise the telescopic boom structure of cranes, achieving a reduction in boom weight and an enhancement in load-bearing capacity. Mijailović and Kastratović [5] analysed various boom cross-sections with mass minimisation as the optimisation goal, applying the Lagrange multiplier method for optimisation, and compared the results with finite element analysis to provide recommendations for the optimal design of boom cross-sections. Wang et al. [6] introduced topology optimisation into the design of crane telescopic boom sections, obtaining a rational section shape. Savkovic et al. [7] analysed the local stresses in the contact area between the inner and outer segments of the telescopic boom of a crane, deriving analytical expressions for the stresses and deformations in the contact area, which offer guidance for the optimal design of the telescopic boom structure. Gašić et al. [8] determined the optimal parametric relationship between the telescopic boom sections of a truck crane to ensure minimisation of the boom mass while satisfying strength and stiffness requirements, employing a solution based on the Lagrange multiplier method combined with the differential evolutionary algorithm, and compared and analysed the two algorithms. Hong and Lee [9] used a three-factor experimental design approach to optimise the shape of the boom connecting shaft based on static analysis, reducing the maximum equivalent force by 32.33% while ensuring the working characteristics of the telescopic boom. Wang and Liu [10] took the change in arm mass and stiffness under the constraints of material yield strength and stiffness as the optimisation objective and utilised the NSGA-II multi-objective genetic algorithm to determine the optimal cross-sectional dimensions of the boom segments, ultimately achieving a lightweight design goal with a 13.3% weight reduction. Liu et al. [11] reduced the mass of the boom by establishing a parametric model of the telescopic boom of a truck-mounted crane and combining finite element analysis and numerical optimisation to carry out multi-objective optimisation of the boom mass and deflection. Wang et al. [12] optimised the crane's main girder design through the particle swarm optimisation algorithm, reducing the mass of the main girder by 6% while ensuring overall structural stability. Zhang et al. [13] focused on the extended boom U-section and optimised the thickness of the cover plate and web plate on the extended arm section using finite element software, achieving a weight reduction rate of 15.2%. Wang and Xing [14] used a truck crane as a research subject and applied the response surface method to optimise the key cross-section parameters of the telescopic boom under hazardous working conditions to achieve a lightweight design.

From existing research, scholars have extensively studied the telescopic boom, providing significant references for improving performance. However, few studies have focused on multi-level optimisation for the telescopic boom cross-section, and most utilise a single optimisation method. This paper takes a specific type of forklift truck boom as the research subject, employing a topology optimisation method based on the variable density approach to achieve the optimal cross-sectional shape during the conceptual design phase. Building on this, parametric modelling of the telescopic boom is carried out, based on the post-topology reconstruction cross-sectional model, further improving the telescopic boom design through parameter optimisation, aiming to minimise material usage while meeting performance requirements and achieving a lightweight design for the boom and the entire machine.

2. Conceptual Design of the Telescopic Boom Cross-Section

2.1 Forklift boom structure analysis

The forklift boom studied in this paper is a telescopic structure with a large span and high strength, capable of multi-angle handling, as shown in Fig. 1. The basic boom is supported by the ear plate and the luffing cylinder, the boom-to-boom contact is achieved by means of sliders, and the rotary table is articulated to the basic boom by means of a pin. Under full extension, the boom extends to a total length of approximately 10.8 metres.

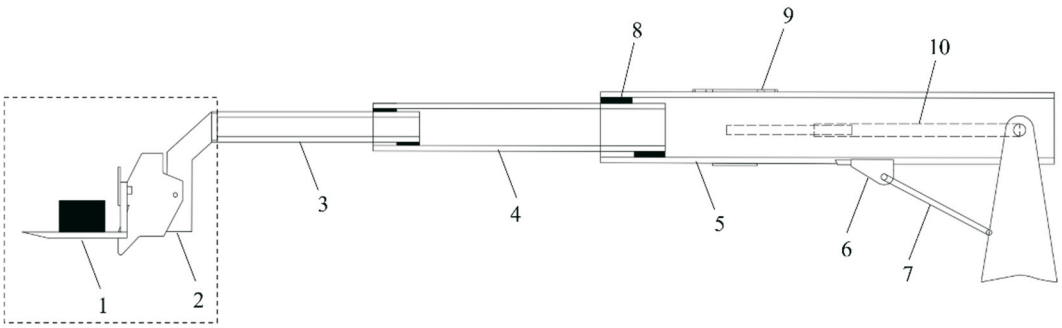

1 pallet fork; 2 lifting boom; 3 outer boom; 4 intermediate boom; 5 basic boom; 6 ear plate; 7 luffing cylinder; 8 slider; 9 reinforcement plate; 10 telescopic cylinder

Fig. 1 Forklift truck boom overall structure

2.2 Establishing the finite element model of the telescopic boom cross-section

The telescopic forklift boom can extend to a maximum length of 10 metres, while the shortest section of the boom measures nearly 4 metres, which makes the telescopic boom prone to flexural buckling [15]. If topology optimisation is performed for the whole section of the boom, it will lead to a large amount of computation, and it is difficult to obtain the ideal cross-section shape. In addition, when the boom is working, the three sections of the boom jointly bear the external load, the force situation is complicated, and the initial boundary conditions are difficult to determine. Therefore, analysing one section of the boom alone is not suitable. The ideal method is to select for analysis a section of the boom structure with a length of 0.5 to 1 times the height of the telescopic boom section from the instability half-wave section near the critical section.

The fully extended telescopic boom is selected as the object of analysis. The rectangular cross-section model of the boom is meshed, with its dimensions shown in Fig. 2(a). The displacement constraints in the x, y, and z directions, along with the rotation constraints in the y and z directions, are applied at one end of the telescopic boom. Correspondingly, loads are applied at the other end according to actual working conditions, thereby completing the establishment of the finite element model of the boom's cross-section, as shown in Fig. 2(b).

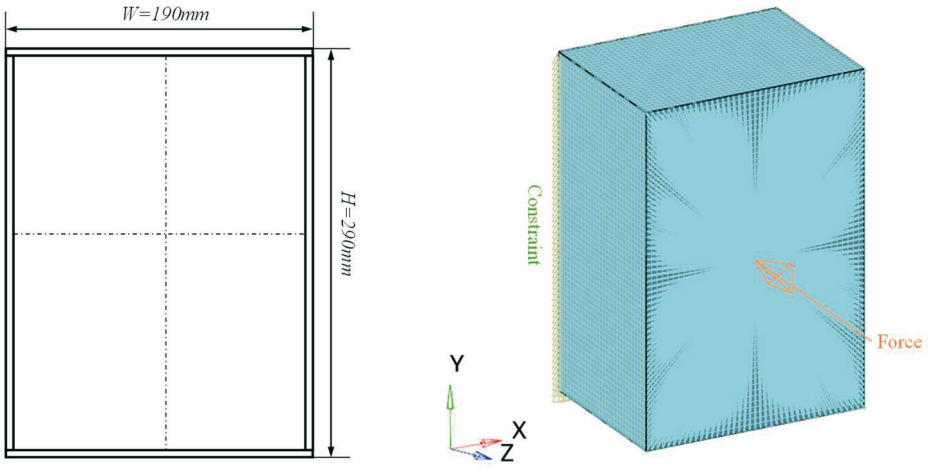

(a) Section size (b) Cross-sectional finite element model

Fig. 2 Schematic diagram of the boom section optimisation model

Loads are calculated on the cross-section model, evaluating two working conditions: one scenario involves the forklift boom under axial force only, and the other involves the boom subjected to axial force, tangential force, and bending moment, as depicted in Fig. 3. F_N, F_T, and M_X denote the axial force (7500N), tangential force (12,990N), and moment (6125 $N \cdot m$) applied to the head of the boom, respectively.

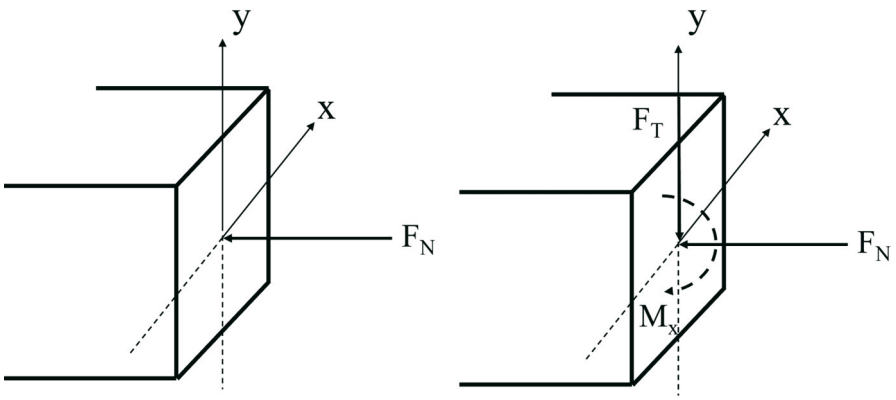

(a) Force sketch I (b) Force sketch II

Fig. 3 Schematic diagram of forces for various working conditions

2.3 Topology optimisation mathematical model of the telescopic boom section

In this paper, a cross-section of a forklift boom from an enterprise is selected as the object of study. The boom frame's cross-section is quadrilateral, and each section consists of a top plate, a bottom plate, and two side plates. Despite the maturity of the currently adopted right-angled rectangular section in manufacturing, it has deficiencies in mechanical properties, especially when subjected to multidirectional complex loads. Stress concentration tends to occur at the corners, which affects its durability. To enhance the load-carrying capacity of the telescopic boom and prolong its service life, it is proposed to use the topology optimisation method to carry out an innovative design of the telescopic boom cross-section.

Topology optimisation of the telescopic boom cross-section is carried out using the variable density method, with the objective of ensuring maximum stiffness of the structure and finding the optimal form of arrangement of the materials. To avoid singular solutions during the optimisation process, a type of brittle material is typically filled in, and the range of variation

for the element density x_i is set to $x_{\min} \le x_i \le 1$, where material with a density less than $x_{\min}$ can be removed [16]. With the minimum flexibility of the structure as the objective, and the volume fraction of structural elements as the constraint, the topology optimisation mathematical model for the boom section is established as follows:

$$\begin{aligned} &Find: && \boldsymbol{x} = \left(x_1, x_2, \cdots\cdots, x_n\right)^T \\ &Minimise: && \boldsymbol{C} = \boldsymbol{F}^T \boldsymbol{U} \\ &Subject: && f = \frac{V_1}{V_0} \\ & && \boldsymbol{F} = \boldsymbol{K}\boldsymbol{U} \\ & && 0 < x_{\min} \le x_i \le 1 \left(i = 1, 2, \cdots\cdots, n\right) \end{aligned} \tag{1}$$

where $\boldsymbol{x}$ represents the design variable, which is the vector of relative densities for each unit; x_n is the relative density of the n-th unit; $\boldsymbol{F}$ is the load vector; $\boldsymbol{K}$ is the overall stiffness matrix; $\boldsymbol{U}$ is the overall displacement matrix; $x_{\min}$ is the minimum value of the relative material density; f is the volume fraction; V_1 is the optimised structural volume; V_0 is the initial structural volume; and $\boldsymbol{C}$ is the flexibility matrix.

2.4 Optimisation of the cross-section topology with different parameters

Based on a rectangular cross-section solid model, the effects of parameters such as element size, volume fraction, and threshold on the optimisation results under axial force are analysed in this study. The impact of complex loading conditions on the results is minimised by this approach, and the topology optimisation process is accelerated.

2.4.1 The impact of different element sizes on topological maps

Under otherwise identical conditions, the optimisation results of the cross-section topology are affected by element size. Computation time is reduced by larger element sizes, but the results become less distinct and the boundaries less defined; the accuracy of the results is improved by smaller sizes, but the calculation time is longer. Therefore, stable optimisation results of the cross-section topology require a reasonable choice of element size. With the control variable method, the upper limit of the volume fraction is set at 0.4, and three different types of element sizes are considered: 3 mm, 5 mm, and 10 mm. The optimisation results for the cross-section with different element sizes are shown in Fig. 4.

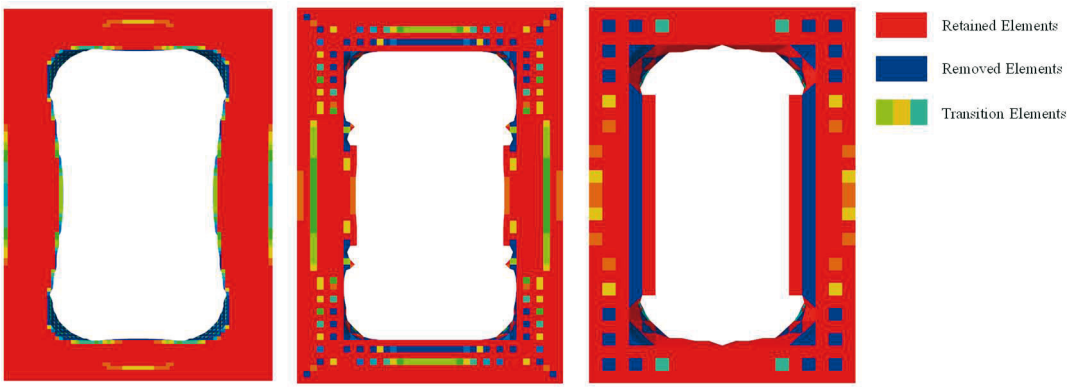

(a) Element size 3 mm (b) Element size 5 mm (c) Element size 10 mm

Fig. 4 Topological configuration of cross-sections with different element sizes

When other conditions remain constant, a smaller element size is chosen to improve the analysis accuracy and to obtain clearer cross-section topology results, which facilitates subsequent model extraction and repair. Specifically, the computation for Fig. 4(a) is approximately 4 hours, for Fig. 4(b) it is approximately 1.5 hours, and for Fig. 4(c) approximately 15 minutes, indicating that reducing the element size significantly increases the topological analysis time. Considering the computational time consumed and the quality of the topological results, the 5.0 mm element size is selected as a reasonable amount and serves as the basis for subsequent analyses. This paper utilises the OptiStruct solver and executes the simulation on a laptop equipped with an AMD Ryzen 7 6800H with Radeon Graphics @ 3.20 GHz and 16 GB RAM.

2.4.2 The impact of different volume fractions on topological maps

The maximum material retention within the design space is defined by the volume fraction constraint. Unnecessary material may be retained by an excessively high volume fraction, while essential material might be removed by an excessively low fraction, resulting in an incomplete topological map, which is unfavourable for subsequent manufacturing. Therefore, an appropriate volume fraction is key for achieving a desirable topological configuration with a uniform element size. The control parameters and conditions are as follows: the element size is uniformly set at 5 mm, the working conditions remain as previously stated, the specific working condition, specifically the scenario of axial loading, is considered, and the upper limits of the volume fractions are 0.1, 0.2, 0.3, 0.5, and 0.7, respectively. The optimisation results for these volume fractions are shown in Fig. 5.

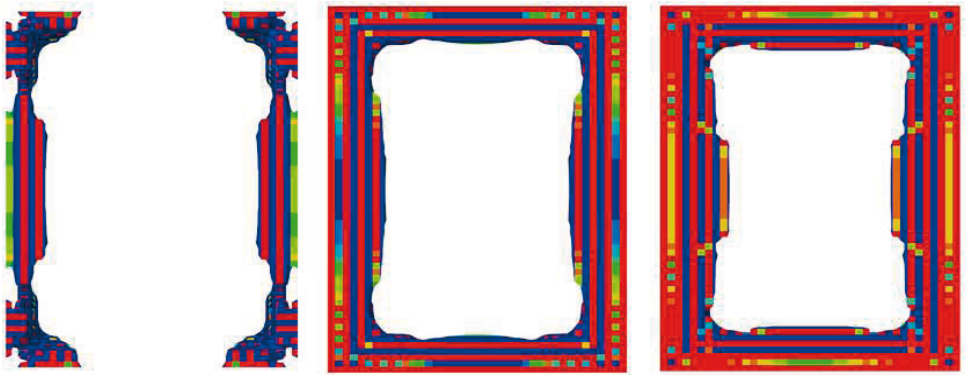

(a) Volume fraction = 0.1 (b) Volume fraction = 0.2 (c) Volume fraction = 0.3

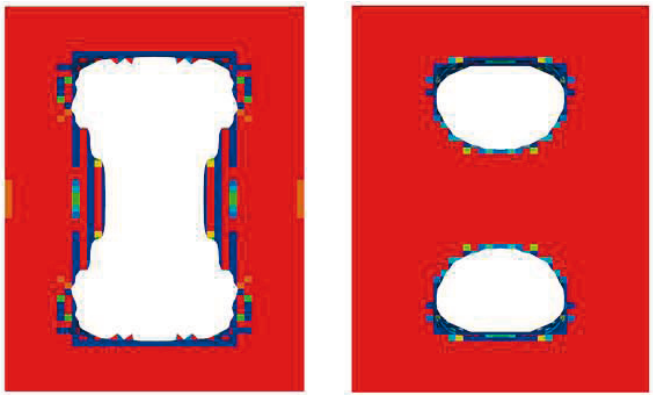

(d) Volume fraction = 0.5 (e) Volume fraction = 0.7

Fig. 5 Topological configuration of cross-sections with different volume fractions

Under identical conditions, the selection of different volume fractions significantly influences the topology optimisation results, as shown in Fig. 5. When subjected to axial force, the main load-bearing parts are the two webs. Fig. 5(b) and Fig. 5(c) demonstrate a more optimal topological shape and are more in line with the machining process, while Fig. 5(c) retains slightly more material, which does not fully demonstrate a reasonable distribution of the material. Excessive material retention in Fig. 5(d) and Fig. 5(e) results in a less favourable topology. Therefore, a volume fraction of 0.2 is selected as a reasonable parameter and is used as the basis for subsequent analysis.

2.4.3 The impact of different thresholds on topological maps

Topology optimisation is carried out using the variable density method, with the optimisation variable being the relative density of the cell material (ranging from 0 to 1). Under a volume fraction constraint, cells with higher relative densities are usually retained, but this does not always ensure an optimal solution. For optimal topology to be achieved, a threshold must be set: cells below this threshold are removed, and those above it are retained. The control variables and their constraints are established as follows: the element size is uniformly 5 mm, the working condition is as previously stated, working condition I is selected, and the upper limit of the volume fraction is taken as 0.2. The optimisation results for the cross-section corresponding to different thresholds are shown in Fig. 6.

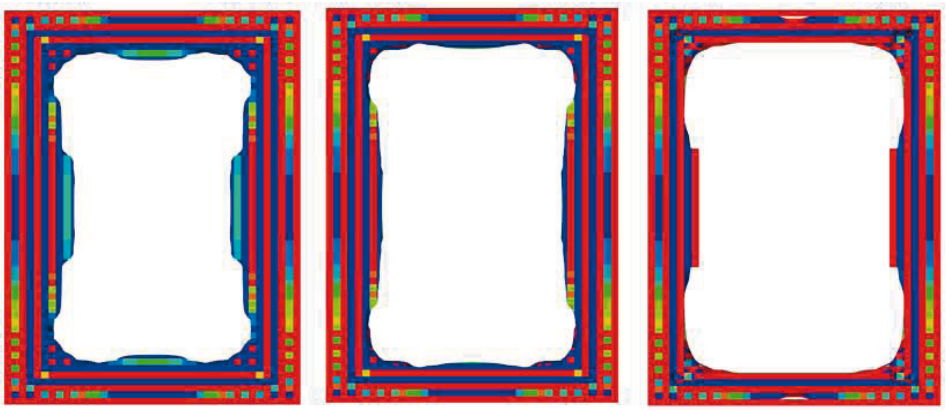

(a) Threshold of 0.1 (b) Threshold of 0.3 (c) Threshold of 0.5

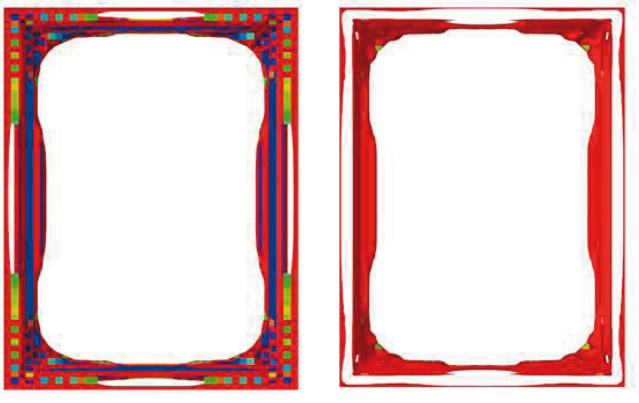

(d) Threshold of 0.7 (e) Threshold of 0.9

Fig. 6 Topological configuration of cross-sections with different thresholds

In Fig. 6, as the threshold value increases, fewer material units are retained, which more accurately reflects the main load-bearing parts, leading to a clearer topology, although the continuity and integrity of the structure are affected. For instance, at a threshold value of 0.9,

the cross-section shape is left unclosed, which does not meet the design and fabrication requirements. However, if the threshold is set too low, as depicted in Fig. 6(a), insufficient material removal occurs, and the manufacturability of the cross-section is poor, limiting its practical value. In summary, a threshold value of 0.5 is most reasonably selected as the preferred value.

2.5 Post-processing for cross-section topology optimisation

The optimal element size, volume fraction, and threshold are determined under conditions of axial force alone. Subsequently, these values are applied to the second condition, which includes axial force, bending moment, and shear force. Topology optimisation is performed on the telescopic boom cross-section to achieve optimised results. Given the irregular nature of the topology-optimised figure and the constraints of practical manufacturing processes, the design is refined and reconstructed using 3D modelling software. Eventually, an optimised cross-section that meets the requirements is obtained. The optimised cross-section, which is depicted as a small, rounded rectangle, features arc transitions that connect the upper and lower flange plates with the sides of the web. This design prevents stress concentration at the corners, enhances stability, and more effectively utilises the material's mechanical properties. The entire post-processing workflow is shown in Fig. 7.

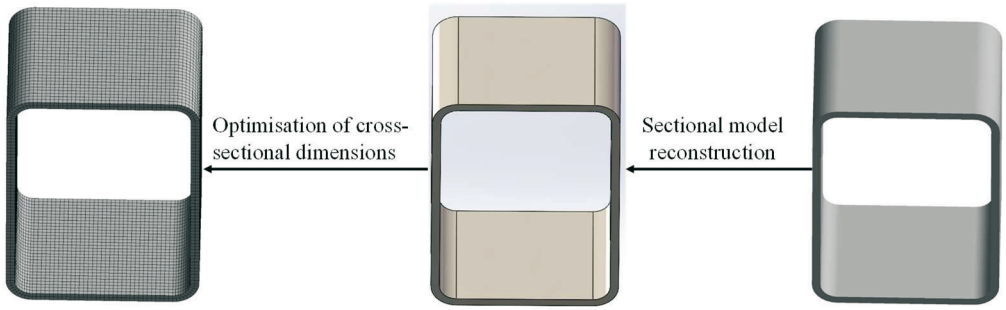

Fig. 7 Post-processing flow for cross-section topology optimisation

3. Static analysis of the telescopic boom

3.1 Finite element model of the telescopic boom

A three-dimensional model of the telescopic boom for a forklift truck is created using SolidWorks software and then imported into ANSYS finite element software. The boom body is made of Q345 steel, while the slider is made of MC nylon, which has good wear resistance and excellent mechanical strength. The specific material properties are shown in Table 1. To ensure mesh quality, non-critical features such as pins and holes are simplified prior to the establishment of the finite element model.

Table 1 Material properties

Components	Material name	Density / (kg · m^{-3})	Young's modulus / MPa	Poisson's ratio
Telescopic boom	Q345 steel plate	7850	2.06×10^5	0.3
Sliders	MC Nylon	1160	4×10^3	0.4

SOLID187 elements are utilised for meshing the telescopic boom, as they can more accurately simulate the stress distribution in the plate thickness direction. To ensure the independence of the simulation results, it is necessary to determine an appropriate mesh size through mesh-independence analysis that meets the accuracy requirements without wasting computational resources [17].

The boom's stress and deformation under a 30° working condition are calculated using various maximum element sizes, as shown in Fig. 8. It is observed that when the maximum element size is set to 20 mm, the maximum equivalent stress and deformation stabilise. After local mesh refinement is performed around areas susceptible to stress concentration, the final finite element model of the boom is established, as shown in Fig. 9. This model consists of 251,847 elements and 505,888 nodes, with an average mesh quality of 0.74607, which signifies excellent mesh quality. Since the analysis in this paper is based on a specific operational posture at a given moment where there is no relative displacement between the boom sections, the contact between the slider and the boom body is simulated using a rigid connection.

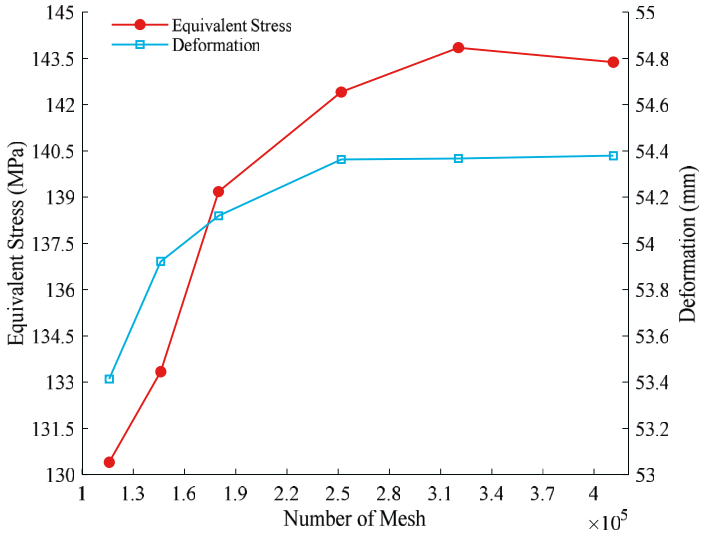

Fig. 8 Grid independence analysis

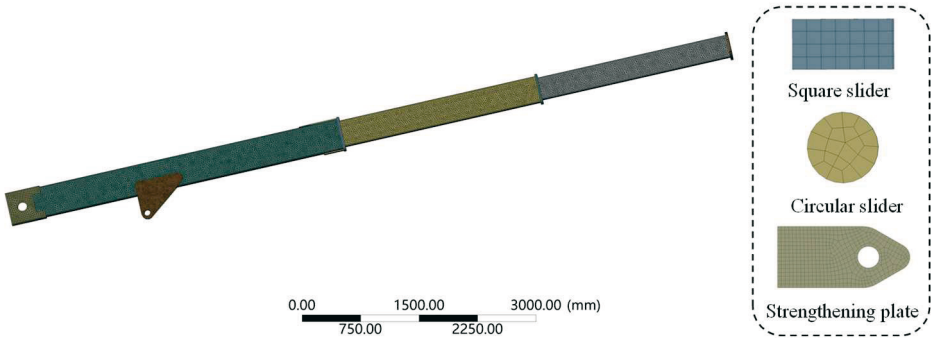

Fig. 9 Gridded model of the telescopic boom

In the 30° elevation handling condition, both the intermediate and outer segment booms of the telescopic boom forklift truck are extended simultaneously, and the boom mainly bears the self-weight G_H and the maximum load G_3 in the luffing plane. During operation, the forklift boom supports the load through the fork. Consequently, it is essential to transfer the load from the fork to the end cap of the outer segment boom. In the process, it is also necessary to consider the weight of the fork and the lifting boom, with gravity forces denoted as G_2 and G_1, respectively. According to the force translation theorem, an equivalent moment M_x must be applied to the end cap of the outer segment boom. The calculation sketch is shown in Fig. 10, and the calculation proceeds as follows:

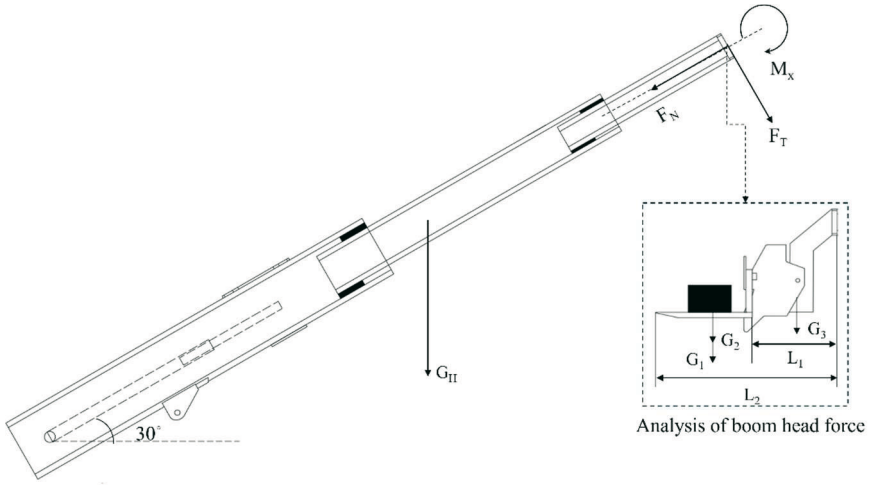

Fig. 10 Sketch of force on the telescopic boom

$$\text{Rated lifting load: } F_s = \left(G_1 + G_2 + G_3\right) g \tag{2}$$

The rated lifting load is decomposed into axial force and radial force within the variable amplitude plane, where the axial force is:

$$F_N = F_s \sin 30° \tag{3}$$

$$\text{The radial force is: } F_T = F_s \cos 30^{\circ} \tag{4}$$

$$\text{Equivalent moment: } M_X = \frac{1}{2} L_1 \times G_2 + \frac{1}{2} L_2 \times \left(G_1 + G_3\right) \tag{5}$$

where L_1 is the horizontal distance from the lifting boom to the boom head and L_2 is the horizontal distance from the fork to the boom head.

After determining the forces on the telescopic boom under 30° working conditions, constraints are subsequently applied. The root of the basic boom is hinged to the base using a pin. At the hinged connection between the basic boom and the lifting cylinder, remote constraints are applied to control the *Z*-axis and *Y*-axis, which limit displacement along the *X*-axis while allowing rotation, as shown in Fig. 11.

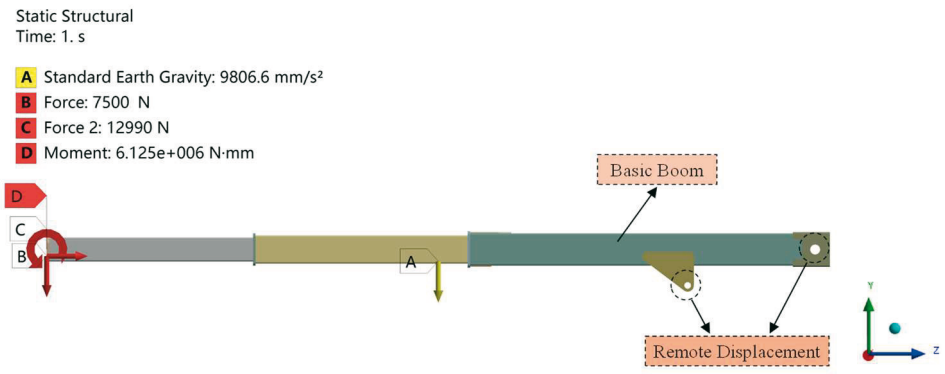

Fig. 11 Loads and boundary conditions

3.2 Results of the static mechanical analysis

The maximum permissible stress is determined by the yield limit of the material and the safety factor. The material of the telescopic boom in the paper is Q345 steel, indicating that its yield limit is 345 MPa. As there are no design guidelines for a forklift boom in China, and its

boom is analogous to that of the crane, referring to the GBT3811-2008 Cranes Design Code, the safety factor $n = 1.35$ can be selected, and the maximum permissible stress is finally determined as follows:

$$[\sigma] = \frac{\sigma_s}{n} = \frac{345}{1.35} = 255.6 \text{ MPa} \tag{6}$$

where σ_s is the yield limit of Q345 material and n is the safety factor.

During operation, significant deformation is experienced by the boom due to various loading conditions. Oscillation may result from excessive deformation, affecting the stability and safety of the operation. In accordance with the GBT3811-2008 Crane Design Code, the relationship between the allowable deflection of the telescopic boom and its length is determined as follows:

$$[Y] \leq \frac{L_C^2}{1000} \tag{7}$$

where $[Y]$ is allowable deflection and L_C is the length of the telescopic boom.

Under the aforementioned conditions, the finite element simulation results for the telescopic boom are shown in Fig. 12. The stress and deformation cloud diagram shows that the maximum stress within the boom, reaching 142.41 MPa, occurs at the connection between the basic and intermediate booms and is considerably lower than the allowable stress. The total deformation, amounting to 54.363 mm, is observed at the end cover of the telescopic boom, which aligns well with practical expectations. Under the condition of satisfying structural strength and stiffness, the boom has a large optimisation space, and therefore the cross-section parameters of the telescopic boom can be optimised.

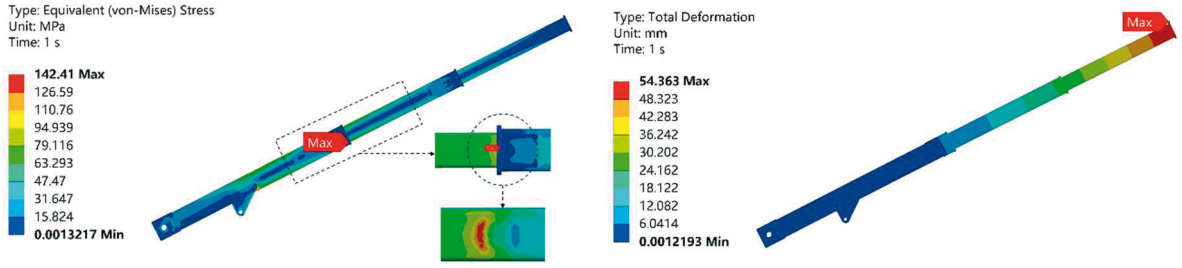

(a) Stress distribution (b) Displacement distribution

Fig. 12 Before optimisation telescopic boom performance distribution diagram

3.3 Telescopic boom structure optimisation process

To further enhance the mechanical performance of the forklift telescopic boom, this paper combines the Kriging surrogate model with the MOGA algorithm to perform parameter optimisation on the boom cross-section. The specific optimisation process is shown in Fig. 13. First, the telescopic boom's parametric model is reconstructed based on the obtained optimal cross-sectional topology configuration, and its static characteristics are analysed using finite element analysis. Then, the optimal space-filling sampling method is employed to generate sample points for the design variables, and the Kriging method is utilised to construct a high-precision surrogate model. Finally, the MOGA algorithm is applied to optimise and obtain the optimal cross-sectional size parameters of the telescopic boom.

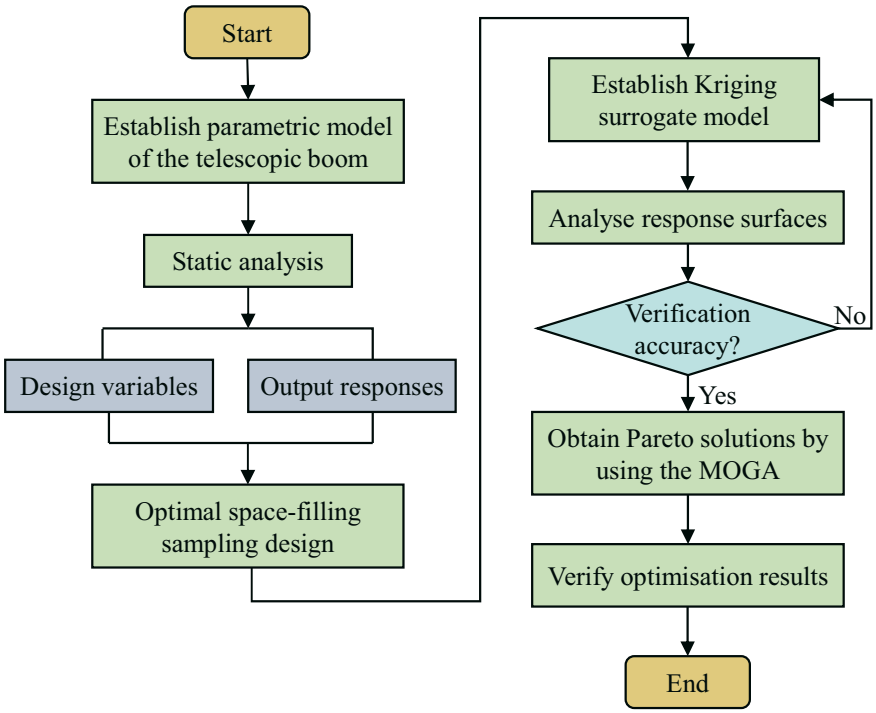

Fig. 13 Optimisation flow chart

4. Parameter optimisation of telescopic boom cross-section

4.1 Establishment of optimisation mathematical model

The primary objective of the telescopic boom cross-section optimisation is to achieve a lightweight design, which entails reducing mass while still meeting the requirements for strength and stiffness. The telescopic boom of the forklift truck consists of three sections, and the optimal cross-sectional shape is determined to be a small, rounded rectangle through the application of topology optimisation. The cross-sectional parameters for each section of the boom are shown in Fig. 14.

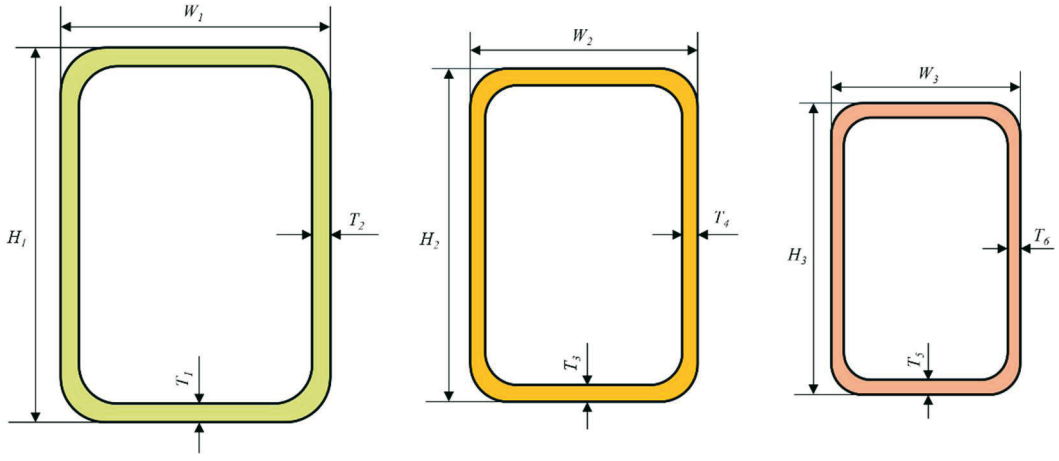

(a) Basic boom (b) Intermediate boom (c) Outer boom

Fig. 14 Schematic of cross-sectional dimensions for each boom section

As shown in Table 2, the height and width of the basic boom section, the thickness of the upper and lower cover plates, the thickness of the left and right side plates, and the thickness of the other two boom sections are used as design variables to optimise the

telescopic boom section parameters. Using the equation function of the 3D modelling software, the cross-sectional dimensions of the other section booms are correlated with the cross-sectional dimensions of the basic boom, thus avoiding interference between the height and width of the booms during subsequent optimisation. With the mass (M), maximum deformation (T), and equivalent stress (S) of the telescopic boom as objective functions, and with the deformation of the telescopic boom limited to 83.7 mm, and the maximum equivalent stress not exceeding the material's permissible stress of 255.6 MPa, the optimised mathematical model is established as follows:

$$\begin{aligned} &Find: && \boldsymbol{x} = (H_1, W_1, T_1, T_2, T_3, T_4, T_5, T_6)^T \\ &Minimise: && \{F(\boldsymbol{x}), S(\boldsymbol{x}), T(\boldsymbol{x})\} \\ &Subject: && S(\boldsymbol{x}) - [\sigma] \le 0 \\ & && T(\boldsymbol{x}) - [Y] \le 0 \end{aligned} \tag{8}$$

where $\boldsymbol{x}$ represents the optimised design variable and $F(x), T(x), S(x)$ represent the mass, maximum deformation, and maximum equivalent stress, respectively.

Table 2 The variation ranges of the telescopic boom size parameters

Serial number	Size parameters	Initial value/mm	Range of change/mm
1	P1-H_1	390	351-429
2	P2-W_1	290	261-319
3	P3-T_1	10	8-12
4	P4-T_2	10	8-12
5	P5-T_3	10	8-12
6	P6-T_4	10	8-12
7	P7-T_5	10	8-12
8	P8-T_6	10	8-12

4.2 Optimal space-filling sampling design

Design of Experiment (DOE) involves the systematic arrangement of experimental methods to observe changes in responses by continuously varying design variables. Compared to other experimental design methods such as Full Factorial Design and Central Composite Design (CCD), the Optimal Space-Filling (OSF) method can significantly reduce the number of experiments required while ensuring spatial coverage, making it particularly suitable for optimisation problems with high-dimensional variables and high computational costs for simulations. The basic principle of the OSF sampling method is to uniformly select sample points throughout the design space and allow for customisation of the number of samples [18]. This method effectively collects design information from different regions, has good projection characteristics, and thus lays the foundation for constructing a high-precision response surface model. Fig. 15 shows the distribution of sample points for design variable P1 under CCD and OSF experimental methods with the same number of samples. The comparison indicates that the distribution of sample points is more uniform and achieves better space-filling when using the OSF method. Hence, the OSF method is chosen for sampling.

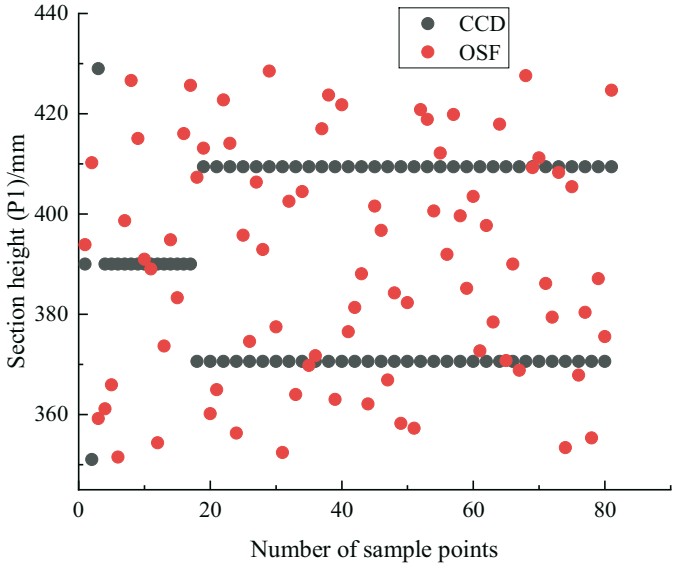

Fig. 15 CCD and OSF design sample points

Taking the eight structural parameters of the telescopic boom cross-section as design variables, experimental samples are generated using the OSF method based on the maximum entropy principle [19]. The number of sample points required to construct a surrogate model is typically about ten times the number of variables. Therefore, this study generated 81 sample points to ensure the spatial uniformity of sampling and the accuracy of the model. The corresponding response values for each sample point are calculated using ANSYS software. The sample points along with their response values are shown in Table 3.

Table 3 Optimal space-filling sampling partial sample parameters

No.	Design variables					Output responses		
	P1 / mm	P2 / mm	P3 / mm	…	P8 / mm	P9 / kg	P10 / mm	P11 / MPa
1	351.48	284.99	11.333	…	9.5556	1225.3	66.599	197.66
2	352.44	307.19	10.543	…	11.877	1276.8	62.783	179.67
3	353.41	311.48	10	…	9.4074	1158.2	68.314	181.37
4	354.37	274.96	8.8642	…	11.728	1135.6	74.368	194.39
…	…	…	…	…	…	…	…	…
78	425.63	283.56	11.086	…	11.235	1355.6	46.221	136.51
79	426.59	287.14	10.296	…	8.5185	1372.8	45.544	122.71
80	427.56	312.91	9.7037	…	10.099	1452.8	42.416	126.59
81	428.52	292.15	9.3086	…	10.296	1307.1	45.669	126.03

4.3 Response surface fitting

In engineering, the methods for response surface fitting include a genetic algorithm for fitting, non-parametric regression fitting, standard response surface full quadratic polynomial fitting, neural network fitting, and Kriging fitting. The accuracy of the fitting surface is typically assessed by the determination coefficient R^2, where the closer R^2 is to 1, the better the fit of the model, indicating a more precise relationship between the objective function and the design variables [20]. The formula is given by:

$$R^2 = 1 - \frac{\sum_{i=1}^{m}\left(y_i - \hat{y}_i\right)^2}{\sum_{i=1}^{m}\left(y_i - \bar{y}\right)^2} \tag{9}$$

where y_i represents the response value corresponding to the i-th sample point and $\hat{y}_i$ represents the predicted value obtained from the response surface model.

Based on the experimental sample points from the optimal space-filling design, the response surface model is fitted using the above five fitting methods, respectively. The determination coefficients (R^2) are detailed in Table 4.

Table 4 Determination coefficients of different fitting methods

Name	Mass coefficient of determination R^2_M	Maximum deformation coefficient of determination R^2_T	Maximum equivalent stress coefficient of determination R^2_S
Genetic clustering algorithm	1	0.99949	0.88723
Non-parametric regression	0.9982	0.99871	0.99823
Standard response surface	1	0.99999	0.94229
Neural network	0.99795	0.99961	0.81973
Kriging	1	1	1

The determination coefficient of the response surface model's accuracy indicates that the experimental points generated by the optimal space-filling design method are accurately matched by the Kriging method, yielding an efficient and accurate response surface model. Thus, the response surface is fitted using the Kriging method, with the expression provided below:

$$\bar{y}(x) = g(x) + z(x) \tag{10}$$

$$g(x) = \beta_0 + \sum_{\mathrm{i}=1}^{\mathrm{k}}\beta_{\mathrm{i}}x_{\mathrm{i}} + \sum_{\mathrm{i}=1}^{\mathrm{k}}\beta_{ii}x_i^2 + \sum_{\mathrm{i}=1}^{\mathrm{k}}x_{\mathrm{i}}\sum_{\mathrm{j}=1}^{\mathrm{k}}\beta_{ij}x_{\mathrm{j}} \tag{11}$$

where $g(x)$ represents the polynomial function; k represents the number of variables; $\beta_0, \beta_i, \beta_{ii}, \beta_{ij}$ are unknown constants.

$z(x)$ is a stochastic process that follows a normal distribution with variance σ^2 and an expected value of 0. However, the covariance is non-zero, which means that $z(x)$ is not independent, but is identically distributed. The covariance matrix of $z(x)$ is:

$$Cov\left[z\left(x^i\right), z\left(x^j\right)\right] = \sigma^2 \boldsymbol{R}\left(\left[\mathrm{r}\left(x^i, x^j\right)\right]\right) \tag{12}$$

Where σ^2 represents the variance of $z(x)$; $\boldsymbol{R}$ is the correlation matrix; and $r\left(x^i, x^j\right)$ is the Gaussian correlation function.

The Gaussian function is recognised as the most effective and widely adopted. It is particularly suitable for modelling highly nonlinear functions. The Gaussian correlation function is:

$$r\left(x^i, x^j\right) = \exp\left(-\sum_{i=1}^{k} \theta_l \left|x_l^i - x_l^j\right|^2\right) \tag{13}$$

where k represents the number of variables; θ_i represents the correlation parameters; and x_l^i, x_l^j represent the i-th and j-th components of the sampling points x^i, x^j.

Optimisation with the Kriging surrogate model requires setting up validation points, a total of three, as a comparison to the predicted values, as shown in Fig. 16. The fit is assessed by how close the points are to the $y=x$ line, with closer points indicating a better fit. As can be seen from the figure, the predicted values of mass, deformation, and stress are well fitted to the design points. The deformation and mass validation points are well fitted, but the three stress (P11) validation points are poorly fitted.

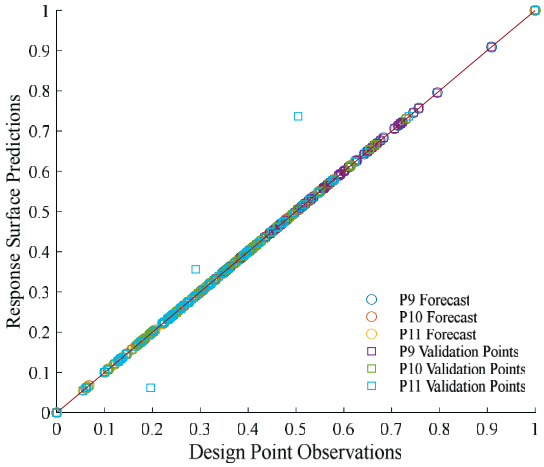

Fig. 16 Fitting curve

Design variables significantly impacting the telescopic boom's mass, stress, and deformation are identified by sensitivity analysis [22]. In Fig. 17, among the eight design variables, P1, P2, P4, and P6 are found to significantly influence quality (P9), P1 and P3 significantly influence deformation (P10), and P1 and P5 impact stress (P11). Consequently, response surfaces are constructed using these significantly impactful design variables to illustrate their impact on mass, deformation, and stress.

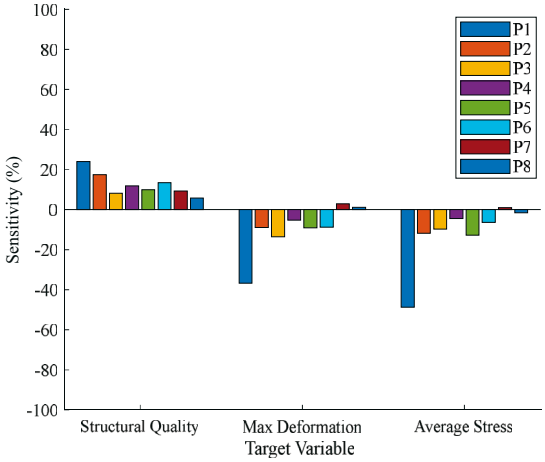

Fig. 17 Sensitivity analysis

The Kriging surrogate model is applied to fit the response surface. The created response surface model is shown in Fig. 18.

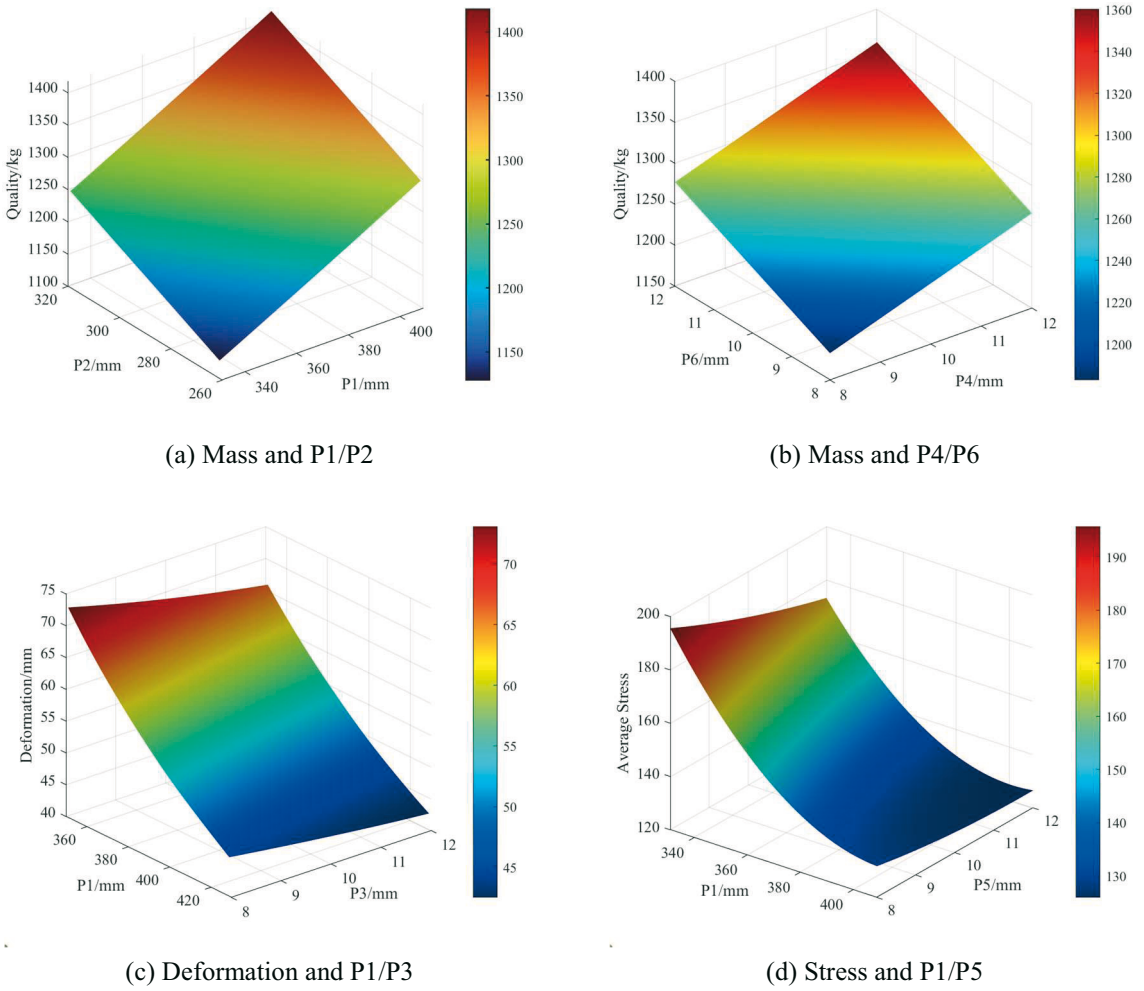

(a) Mass and P1/P2

(b) Mass and P4/P6

(c) Deformation and P1/P3

(d) Stress and P1/P5

Fig. 18 Design variables and output responses curved surface diagrams

From Fig. 18(a), it is observed that as P1 and P2 increase, the mass of the telescopic boom first increases and then decreases, reaching a minimum at P1 = 351 mm and P2 = 261 mm. As shown in Fig. 18(b), P4 and P6 have linear relationships with mass, resulting in an overall flat response surface. In Fig. 18(c), the telescopic boom's deformation increases and then decreases as P1 and P3 increase, with maximum deformation occurring when P1 and P3 are at their minimum values. As shown in Fig. 18(d), the stress of the telescopic boom decreases as the P1 and P5 dimensions increase, decreasing significantly with the increase of P1 and gradually with the increase of P5. Stress does not vary linearly with these design variables, explaining the poor fit of the stress validation points. The telescopic boom's stress is at its maximum when P1 is at its maximum and P5 at its minimum.

4.4 Multi-objective genetic algorithm (MOGA) optimisation

The Multi-Objective Genetic Algorithm (MOGA) is an optimisation algorithm used to find Pareto optimal solutions, aiming to achieve balanced solutions among multiple conflicting objective functions. Fig. 19 shows the flowchart of the MOGA algorithm, whose core idea is based on Pareto ranking and niche technology, enhancing population diversity and preventing premature convergence by searching for the Pareto optimal front. Compared to screening algorithms, MOGA is more suitable for global search, offers higher computational efficiency, requires no specified initial points, and is easier to implement [23]-[24].

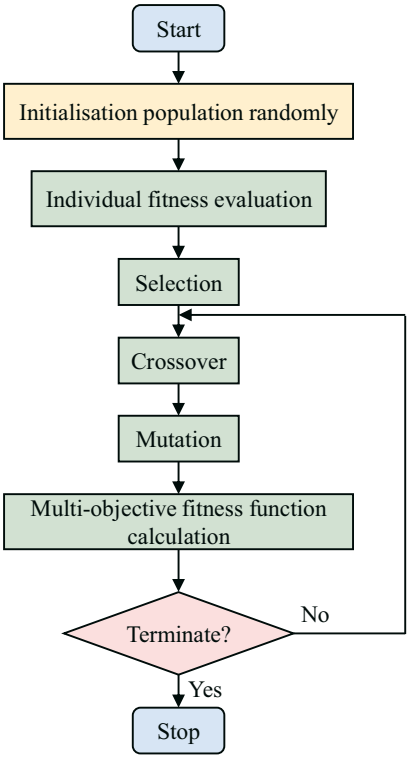

Fig. 19 MOGA algorithm flow chart

The decision-making process (DMP) is a technique used for sorting Pareto optimal samples. Its core is to define a global aggregation objective function ϕ, and calculate this function using the fuzzy evaluation combined with the Monte Carlo sampling method to determine the optimal solution. The specific expression is as follows:

$$\phi = \sum_{i=1}^{n} w_i N_i + \sum_{j=1}^{m} w_j M_j + \left(\sum_{f=1}^{l} w_f P_f \right) \tag{14}$$

$$w_i = w_j = \begin{cases} 1.0, \text{ Importance} = \text{Higher} \\ 0.666, \text{ Importance} = \text{Default} \\ 0.333, \text{ Importance} = \text{Lower} \end{cases} \tag{15}$$

where i, j are continuous variables and f is a discrete variable.

Here, we focus primarily on changes in mass. Therefore, mass is selected as “Higher”, while the maximum equivalent stress and total deformation are set to “Default”.

Based on the established Kriging surrogate model, the MOGA algorithm is applied to perform optimisation. The parameters of the MOGA algorithm are set as shown in Table 5. Convergence is achieved after 26,774 iterations, and the set of Pareto optimal solutions obtained through multiple iterations is shown in Fig. 20. After the MOGA algorithm converges, the system automatically selects three sets of points with the best performance as candidate points, as shown in Table 6. It can be observed that all three optimisation schemes can meet the expected optimisation requirements in practical applications. Among the three candidate points, since candidate point 1 has the smallest boom mass, and its equivalent stress and deformation values are not significantly different from the other two candidate points, point 1 is chosen as the final optimisation solution.

Table 5 Parameter configuration for the MOGA

Name	Initial sample size	Each iteration sample size	Maximum allowed Pareto percentage/%	Stable convergence percentage/%	Maximum number of iterations
Numerical value	8000	1600	70	2	20

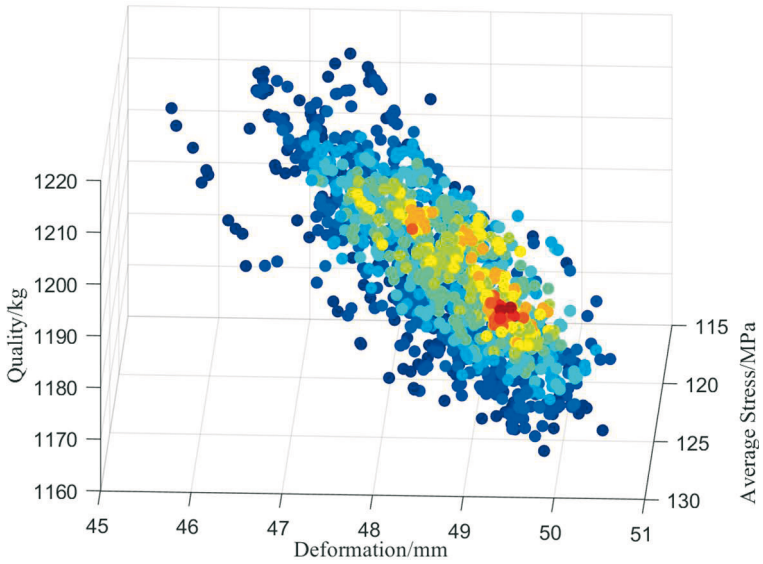

Fig. 20 Pareto optimal solution

Table 6 Optimisation results of input and output variables

Parameter	Candidate point 1	Candidate point 2	Candidate point 3
P1 / mm	412.87	418.12	415.93
P2 / mm	261.07	261.42	262.12
P3 / mm	11.254	11.227	11.283
P4 / mm	8.0422	8.0377	8.0147
P5 / mm	11.777	11.452	11.869
P6 / mm	8.0776	8.0718	8.0801
P7 / mm	8.1233	8.0251	8.0404
P8 / mm	8.0419	8.0208	8.0728
P9 / kg	1162.4	1164.7	1168.2
P10 / mm	50.439	49.496	49.504
P11 / MPa	125.19	126.24	123.5

4.5 Verification of optimisation results

The boom is constructed by welding steel plates, and the cross-sectional dimensions are typically integers. The cross-sectional dimension parameters for candidate point 1, which are non-standard, do not meet actual manufacturing requirements, necessitating the rounding of each parameter. With the rounded parameters, the finite element model is reconstructed and analysed, and the results are shown in Fig. 21. From the figure, the maximum equivalent stress of the optimised boom is 131.56 MPa, and the maximum deformation is 50.342 mm, meeting the requirements for actual operating conditions.

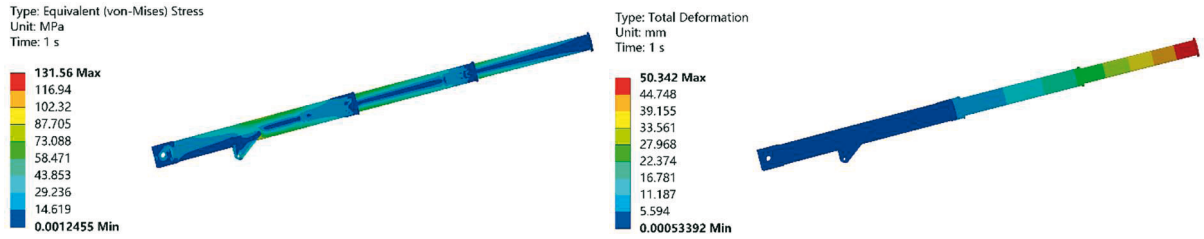

(a) Stress distribution (b) Displacement distribution

Fig. 21 Optimised stress and deformation distribution diagram

A comparative analysis of the forklift truck boom model before and after optimisation is presented in Table 7. The results show that the mass of the optimised boom is reduced by 8.67% compared with the original, the stress and deformation are reduced, and the purpose of the lightweight design is achieved.

Table 7 Comparison of results before and after optimisation

Responses	Before optimisation	After optimisation	Percentage of change
Mass / kg	1271.5	1161.3	8.67%
Total deformation / mm	54.363	50.342	7.39%
Equivalent stress / MPa	142.41	131.56	7.61%

5. Conclusions

To improve the load-bearing capacity and to extend the service life of the telescopic boom for an enterprise, a lightweight design approach based on multi-level optimisation is proposed. A topology optimisation method utilising density interpolation is applied to conceptually design the original telescopic boom cross-section. The optimal cross-section topology is determined by analysing the impact of element size, volume fraction, and threshold on its topology configuration, considering machining processability and structural mechanical properties.

The topology-optimised telescopic boom model is reconstructed, with the optimal space-filling design method employed to generate experimental design sample points. According to the design results, a variety of fitting methods are applied, and the accuracy is verified. It is found that the Kriging method can accurately match the sample points generated by the optimal space-filling experimental design method. The fitted response surface model is highly efficient and accurate. The multi-objective genetic algorithm is utilised for the solving computation, and a set of optimal cross-section size parameters, capable of meeting the actual engineering requirements, are ultimately obtained.

After the optimisation, the telescopic boom model is reconstructed for static analysis. The results indicate that the total mass of the telescopic boom is reduced by 8.67%, the maximum stress is reduced by 7.61%, and the maximum deformation is reduced by 7.39%, making the optimisation clearly effective. The lightweight design of the telescopic boom is achieved while satisfying strength and stiffness requirements.

This study not only provides a method for optimising the design of telescopic booms but also offers new insights for the optimisation of other mechanical structures. The optimisation approach in this study primarily focuses on the static performance of the telescopic boom. However, in practical engineering applications, the telescopic boom is required not only to withstand static loads but also to endure repeated vehicle loads. In subsequent research, based on the method adopted in this study, the objective and constraint functions can be further refined to incorporate factors such as fatigue performance and buckling stability. The optimised results can then be integrated into the entire machine for validation.

Acknowledgments

This research is supported by the National Natural Science Foundation of China General Project (Grant No. 52477227), the Plan of Key Research Projects of Higher Education of Henan Province (Grant No. 24A460024), and the Henan Province Science and Technology Research Project (Grant No. 242102241052). These sources of financial support are gratefully acknowledged.

REFERENCES

[1] Randive, V.; Kamble, P. D. P.; Pawar, P. A. Finite Element Analysis of Inner Boom for 3Tonn Telescopic Forklift. *International Research Journal of Engineering and Technology* **2018**, 5(7), 1367-1372. https://doi.org/10.13140/RG.2.2.36564.91525

[2] Guo, G.; Zhao, Y.; Su, W.; et al. Topology optimization of thin-walled cross section using moving morphable components approach. *Structural and Multidisciplinary Optimization* **2021**, 63, 2159-2176. https://doi.org/10.1007/s00158-020-02792-0

[3] Shimoda, M.; Liu, Y.; Ishikawa, K. Optimum shape design of thin-walled cross sections using a parameter-free optimization method. *Thin-Walled Structures* **2020**, 148, 106603. https://doi.org/10.1016/j.tws.2020.106603

[4] Ji, A.; Chen, C.; L. Peng, L.; et al. Collaborative optimization of NURBS curve cross-section in a telescopic boom. *Journal of Mechanical Science and Technology* **2017**, 31, 3861-3873. https://doi.org/10.1007/s12206-017-0731-y

[5] Mijailović, R.; Kastratović, G. Cross-section optimization of tower crane lattice boom. *Meccanica* **2009**, 44, 599-611. https://doi.org/10.1007/s11012-009-9204-4

[6] Wang, X.; Huang, L.; Gao, Y.; et al. Topological optimization for crane telescopic boom-section. *Journal of Dalian University of Technology* **2009**, 49(3), 374-379. https://doi.org/10.7511/dllgxb200903013

[7] Savković, M.; Gašić, M.; Pavlović, G.; et al. Stress analysis in contact zone between the segments of telescopic booms of hydraulic truck cranes. *Thin-Walled Structures* **2014**, 85, 332-340. https://doi.org/10.1016/j.tws.2014.09.009

[8] Gašić, M. M.; Savković, M. M.; Bulatović, R. R.; et al. Optimization of a pentagonal cross section of the truck crane boom using Lagrange's multipliers and differential evolution algorithm. *Meccanica* **2011**, 46, 845-853. https://doi.org/10.1007/s11012-010-9343-7

[9] Hong, J. M.; Lee, J. H. Optimal design of boom joint for 2.5 ton class aerial lift truck. *Journal of the Korean Society for Precision Engineering* **2018**, 35, 769-775. https://doi.org/10.7736/KSPE.2018.35.8.769

[10] Wang, Z.; Liu, X. Lightweight optimization design of arm frame for aerial work platform based on NSGA-II algorithm. *IOP Conference Series: Materials Science and Engineering* **2020**, 733, 012037. https://doi.org/10.1088/1757-899X/733/1/012037

[11] Liu, H.; Zhou, C.; Yu, G. Multi-objective optimization of telescopic boom section for truck-mounted crane. *Machine Design & Research* **2020**, 36(01), 173-176. https://doi.org/10.13952/j.cnki.jofmdr.2020.0036

[12] Wang, Y.; Ma, C.; Wang, C.; et al. Characteristics analysis and optimization design of bridge crane based on improved particle swarm optimization algorithm. *Journal of Low Frequency Noise, Vibration and Active Control* **2023**, 42, 253-271. https://doi.org/10.1177/14613484221118994

[13] Zhang, L.; Yu, J.; Xu, Y.; et al. Structural design and cross-section size optimization of crane reach boom for lightweighting objectives. *Journal of Machine Design* **2023**, 40(6), 124-133. https://doi.org/10.13841/j.cnki.jxsj.2023.06.026

[14] Wang, C.; Xing, B. Optimization of Crane Telescopic Boom Structure Based on Finite Element Software. *SAE International Journal of Materials and Manufacturing* **2023**, 16, 189-201. https://doi.org/10.4271/05-16-02-0015

[15] Ji, M.; Zhang, Q.; Peng, D.; et al. Finite element analysis for local stability of telescopic boom of truck crane. *Transactions of the Chinese Society for Agricultural Machinery* **2004**, 35(6), 48-51. https://doi.org/10.3969/j.issn.1000-1298.2004.06.014

[16] Zhou, Y.; Xu, J.; Qi, W.; et al. Optimised Design of Frame Topology Based on the Exponential Scaling Hierarchy Analysis Method. *Transactions of FAMENA* **2024**, 48(3), 77-93. https://doi.org/10.21278/TOF.483060723

[17] Wei, W.; Peng, F.; Li, Y.; et al. Optimization design of extrusion roller of RP1814 roller press based on ANSYS workbench. *Applied Sciences* **2021**, 11(20), 9584. https://doi.org/10.3390/app11209584

[18] Wang, X.; Tsung, F.; Li, W.; et al. Optimal space-filling design for symmetrical global sensitivity analysis of complex black-box models. *Applied Mathematical Modelling* **2021**, 100, 303-319. https://doi.org/10.1016/j.apm.2021.08.015

[19] Serageldin, A. A.; Radwan, A.; Katsura, T.; et al. Parametric analysis, response surface, sensitivity analysis, and optimization of a novel spiral-double ground heat exchanger. *Energy conversion and management* **2021**, 240, 114251. https://doi.org/10.1016/j.enconman.2021.114251

[20] Polat, M. E.; Ulger, F.; Cadirci, S. Multi-objective optimization and performance assessment of microchannel heat sinks with micro pin-fins. *International Journal of Thermal Sciences* **2022**, 174, 107432. https://doi.org/10.1016/j.ijthermalsci.2021.107432

[21] Jiang, W.; Zhang, Y.; Liu, J.; et al. Multi-objective optimization design for steel-aluminum lightweight body of pure electric bus based on RBF model and genetic algorithm. *Electronic Research Archive* **2023**, 31(4), 1982-1997. https://doi.org/ 10.3934/era.2023102

[22] Zhang, X.; Xu, W.; Li, R.; et al. Study on sustainable lightweight design of airport waiting chair frame structure based on ANSYS workbench. *Sustainability* **2024**, 16(13), 5350. https://doi.org/10.1016/j.ijthermalsci.2021.107432

[23] Zhou, J.; Gao, J.; Wang, K.; et al. Design optimization of a disc brake based on a multi-objective optimization algorithm and analytic hierarchy process method. *Transactions of FAMENA* **2018**, 42(4), 25-42. https://doi.org/10.21278/TOF.42403

[24] Shang, Y.; Shen, J.; Wei, W.; et al. Optimization of ball mill cylinder structure based on response surface optimization module and multi-objective genetic algorithm. *Journal of Mechanical Science and Technology* **2024**, 38(7), 3631-3640. https://doi.org/10.1007/s12206-024-0636-5

Submitted: 07.01.2025

Accepted: 20.12.2025

Zhanpeng Fang[1,2]
Liukai Zhao[1,2]
Yanqiu Xiao*[,1,2]
Jiaqi Qi[1,2]
Guangzhen Cui[1,3]
Lianhui Jia[1,4]
Wei Xiao[1,4]
[1]Collaborative Innovation Center of Intelligent Tunnel Boring Machine, Zhengzhou University of Light Industry, Zhengzhou, 450002, China
[2] Henan New Energy Vehicle Lightweight Design and Manufacturing Engineering Research Center, Zhengzhou University of Light Industry, Zhengzhou, 450002, China
[3]International Joint Laboratory for Intelligent Monitoring and Control of Complex Mechanical Equipment in Henan Province, Zhengzhou University of Light Industry, Zhengzhou, 450002, China
[4]China Railway Engineering Equipment Group Co., Ltd, Zhengzhou, 450016, China
*Corresponding author:
xiaoyanqiu@zzuli.edu.cn